AN ADAPTIVE LOCAL DECONVOLUTION METHOD FOR IMPLICIT LES WITH OPTIMIZED SPECTRAL EDDY VISCOSITY

Stefan Hickel & **Nikolaus A. Adams**
Technische Universität München, Institute of Aerodynamics,
D-85747 Garching, Germany
sh@tum.de, nikolaus.adams@tum.de

J. Andrzej Domaradzki
University of Southern California, Department of Aerospace and Mechanical Engineering,
Los Angeles, CA 90089-1191, U.S.A.
jad@usc.edu

ABSTRACT

The Adaptive Local Deconvolution Method (ALDM) is a new nonlinear discretization scheme designed for Implicit Large-Eddy Simulation (ILES). Free parameters of a solution-adaptive deconvolution operator allow to adjust the numerical truncation error which acts as implicit subgrid-scale (SGS) model. To assign physically appropriate values to these parameters the spectral numerical viscosity is analyzed. By an automatic optimization employing an evolutionary algorithm a set of parameters was found which yields an excellent spectral match for the numerical viscosity with theoretical predictions. Computational results for forced and decaying three-dimensional homogeneous isotropic turbulence show an excellent agreement with theory and experimental data.

INTRODUCTION

We consider LES of turbulent flows which are governed by the Navier-Stokes equations and by the incompressible continuity equation. A finite-volume discretization is obtained by convolution with the top-hat filter $\boldsymbol{G}$

$$\frac{\partial \bar{\boldsymbol{u}}_N}{\partial t} + \boldsymbol{G} * \boldsymbol{\nabla} \cdot \boldsymbol{N}_N(\boldsymbol{u}_N) - \nu \boldsymbol{\nabla} \cdot \boldsymbol{\nabla} \bar{\boldsymbol{u}}_N = -\boldsymbol{G} * \boldsymbol{\nabla} \cdot \boldsymbol{\tau}_{SGS} \quad (1a)$$

$$\boldsymbol{\nabla} \cdot \bar{\boldsymbol{u}}_N = 0 \quad (1b)$$

where an overbar denotes the filtering $\bar{\boldsymbol{u}} = \boldsymbol{G} * \boldsymbol{u}$. The nonlinear term is abbreviated as $\boldsymbol{\nabla} \cdot \boldsymbol{N}(\boldsymbol{u}) = \boldsymbol{\nabla} \cdot \boldsymbol{u}\boldsymbol{u} + \boldsymbol{\nabla} p$, where $\boldsymbol{u}$ is the velocity field and p is the pressure. The employed filter approach (Leonard 1974) implies a subsequent discretization of the filtered equations. The subscript N indicates the resulting grid functions obtained by projecting continuous functions on the numerical grid. This projection corresponds to an additional filtering in Fourier space with a sharp cut-off at the Nyquist wavenumber $\xi_C = \pi/h$, where h is a constant grid spacing. The subgrid-stress tensor

$$\boldsymbol{\tau}_{SGS} = \boldsymbol{N}(\boldsymbol{u}) - \boldsymbol{N}_N(\boldsymbol{u}_N) \quad (2)$$

originates from the discretization of the non-linear terms and has to be approximated by a model for closing eq. (1). To certain extents common explicit models are based on sound physical theories. Solved numerically, however, the discrete approximation of the explicit SGS model competes against the truncation error of the underlying numerical scheme. A theoretical analysis performed by Ghosal (1996) comes to the conclusion that even a fourth-order central difference discretization has a numerical error which can have the same order of magnitude as the SGS model. This fact is exploited for implicit large-eddy simulation where no SGS model terms are computed explicitly. Rather the truncation error of the numerical scheme is used to model the effects of unresolved scales. A recent review on previous implicit LES approaches is provided, e.g., by Grinstein and Fureby (2004).

The Modified Differential Equation (MDE) for an implicit LES scheme is given by

$$\frac{\partial \bar{\boldsymbol{u}}_N}{\partial t} + \widetilde{\boldsymbol{G}} * \widetilde{\boldsymbol{\nabla}} \cdot \widetilde{\boldsymbol{N}}_N(\widetilde{\boldsymbol{u}}_N) - \nu \boldsymbol{\nabla} \cdot \boldsymbol{\nabla} \bar{\boldsymbol{u}}_N = \boldsymbol{0} \quad (3a)$$

$$\boldsymbol{\nabla} \cdot \bar{\boldsymbol{u}}_N = 0 \quad (3b)$$

where $\widetilde{\boldsymbol{u}}_N$ denotes an approximant of the velocity $\boldsymbol{u}_N$. The local Riemann problem is solved by a consistent numerical flux function $\widetilde{\boldsymbol{N}}_N$. The symbols $\widetilde{\boldsymbol{G}}$ and $\widetilde{\boldsymbol{\nabla}}$ indicate that $\boldsymbol{G}$ and $\boldsymbol{\nabla}$ are replaced by their respective numerical approximations. In fact $\widetilde{\boldsymbol{G}} * \widetilde{\boldsymbol{\nabla}}$ can be a nonlinear operator. The truncation error is accordingly

$$\boldsymbol{\mathcal{G}}_N = \boldsymbol{G} * \boldsymbol{\nabla} \cdot \boldsymbol{N}_N(\boldsymbol{u}_N) - \widetilde{\boldsymbol{G}} * \widetilde{\boldsymbol{\nabla}} \cdot \widetilde{\boldsymbol{N}}_N(\widetilde{\boldsymbol{u}}_N) \quad (4)$$

For implicit SGS modeling the discretization scheme is specifically designed so that the truncation error $\boldsymbol{\mathcal{G}}_N$ has physical significance, i.e.

$$\boldsymbol{\mathcal{G}}_N \approx -\boldsymbol{G} * \boldsymbol{\nabla} \cdot \boldsymbol{\tau}_{SGS} \quad (5)$$

THE ALDM APPROACH

With the adaptive local deconvolution method (ALDM) the local approximation $\widetilde{\boldsymbol{u}}_N$ is obtained from a solution-adaptive combination of deconvolution polynomials. Numerical discretization and SGS modeling are merged entirely. This is possible by exploiting the formal equivalence between cell-averaging and reconstruction in finite-volume discretizations and top-hat filtering and deconvolution in SGS-modeling. Instead of maximizing the order of accuracy, deconvolution is

regularized by limiting the degree of local interpolation polynomials and by permitting lower-order polynomials to contribute to the truncation error. Adaptivity of the deconvolution operator is achieved by weighting the respective contributions by an adaptation of WENO smoothness measures. The approximately deconvolved field is inserted into a consistent numerical flux function. Flux function and nonlinear weights introduce free parameters. These allow for controlling the truncation error which provides the implicit SGS model.

The efficiency of this approach is demonstrated by Adams et al. (2004) for 1D conservation laws on the example of the viscous Burgers equation. The extension for the three-dimensional Navier-Stokes equations is detailed in Hickel et al. (2005). The main idea is to split the 3D deconvolution into successive 1D operations. Thereby the nonlinear weights and the deconvolution operators are specific for each velocity component and coordinate direction. However, the requirement of an isotropic discretization implies symmetries on the parameters so that the 3D scheme contains only one additional parameter compared with the 1D case. Integration over transversal directions is approximated by a Gaussian quadrature rule. The continuity equation can be satisfied by a fractional step projection approach, where the pressure is computed from a top-hat filtered Poisson equation with the modified convection term.

MODIFIED DIFFERENTIAL EQUATION ANALYSIS

In the following we analyze the MDE in Fourier space in order to develop a theoretical framework for the evaluation of subgrid dissipation and spectral numerical viscosity of ALDM. We consider the discretization of a $(2\pi)^3$-periodic domain. N is the number of grid points in one dimension and $\xi_C = N/2$ is the corresponding cut-off wave number. Using Fourier transforms the MDE (3) can be written in spectral form as

$$\frac{\partial \widehat{\boldsymbol{u}}_C}{\partial t} + \widehat{\boldsymbol{G}}\ \mathrm{i}\boldsymbol{\xi}\cdot\widehat{\boldsymbol{N}}_C(\widehat{\boldsymbol{u}}_C) + \nu\boldsymbol{\xi}^2\widehat{\boldsymbol{u}}_C = \widehat{\boldsymbol{\mathcal{G}}}_C \tag{6a}$$

$$\mathrm{i}\boldsymbol{\xi}\cdot\widehat{\boldsymbol{u}}_C = 0 \tag{6b}$$

The hat denotes the Fourier transform, i is the imaginary unit, and $\boldsymbol{\xi}$ is the wave-number vector. A physical-space discretization covers contributions to the numerical solution to wavenumbers up to $|\boldsymbol{\xi}| = \sqrt{3}\xi_C$. For consistency with spectral theories of turbulence which implie isotropy wave numbers with $|\boldsymbol{\xi}| > \xi_C$ need to be removed. For this purpose we define

$$\widehat{\boldsymbol{u}}_C(\boldsymbol{\xi}) = \begin{cases} \widehat{\boldsymbol{G}}^{-1}(\boldsymbol{\xi})\ \widehat{\boldsymbol{u}}_N(\boldsymbol{\xi}) & ,\ |\boldsymbol{\xi}| \le \xi_C \\ \boldsymbol{0} & ,\ \text{otherwise} \end{cases} \tag{7}$$

On the represented wave-number range the kinetic energy of the deconvolved velocity is

$$\widehat{E}(\boldsymbol{\xi}) = \frac{1}{2}\widehat{\boldsymbol{u}}_C(\boldsymbol{\xi})\cdot\widehat{\boldsymbol{u}}_C^*(\boldsymbol{\xi}) \tag{8}$$

Multiplying equation (6a) by the complex-conjugate $\widehat{\boldsymbol{u}}_C^*$ of $\widehat{\boldsymbol{u}}_C$ we obtain

$$\widehat{\boldsymbol{G}}\frac{\partial \widehat{E}(\boldsymbol{\xi})}{\partial t} - \widehat{\boldsymbol{G}}(\boldsymbol{\xi})\widehat{T}_C(\boldsymbol{\xi}) + 2\nu\boldsymbol{\xi}^2\widehat{\boldsymbol{G}}\widehat{E}(\boldsymbol{\xi}) = \widehat{\boldsymbol{u}}_C^*(\boldsymbol{\xi})\cdot\widehat{\boldsymbol{\mathcal{G}}}_C(\boldsymbol{\xi}) \tag{9}$$

The nonlinear energy transfer

$$\begin{aligned} \widehat{T}_C(\boldsymbol{\xi}) &= \mathrm{i}\widehat{\boldsymbol{u}}_C^*\cdot\boldsymbol{\xi}\cdot\widehat{\boldsymbol{N}}_C(\widehat{\boldsymbol{u}}_C) \\ &= \mathrm{i}\widehat{\boldsymbol{u}}_C^*(\boldsymbol{\xi})\cdot\overset{3}{\boldsymbol{P}}(\boldsymbol{\xi})\cdot\cdot\int_{|\boldsymbol{\eta}|\leqq\xi_C}\widehat{\boldsymbol{u}}_C(\boldsymbol{\xi})\widehat{\boldsymbol{u}}_C(\boldsymbol{\xi}-\boldsymbol{\eta})d\boldsymbol{\eta} \end{aligned} \tag{10}$$

is the Fourier transform of the nonlinear term. The tensor $\overset{3}{\boldsymbol{P}}(\boldsymbol{\xi})$ is defined by $\overset{3}{P}_{lmn}(\boldsymbol{\xi}) = \xi_m\delta_{ln} - \xi_l\xi_m\xi_n\ |\boldsymbol{\xi}|^{-2}$ (Pope 2000). Finally, we deconvolve eq. (9) by multiplication with the inverse filter coefficient $\widehat{G}^{-1}(\boldsymbol{\xi})$ which is defined on the range of represented scales $|\boldsymbol{\xi}| \leqq \xi_C$ and obtain

$$\frac{\partial \widehat{E}(\boldsymbol{\xi})}{\partial t} - \widehat{T}_C(\boldsymbol{\xi}) + 2\nu\boldsymbol{\xi}^2\widehat{E}(\boldsymbol{\xi}) = \widehat{\boldsymbol{G}}^{-1}(\boldsymbol{\xi})\widehat{\boldsymbol{u}}_C^*(\boldsymbol{\xi})\cdot\widehat{\boldsymbol{\mathcal{G}}}_C(\boldsymbol{\xi}) \tag{11}$$

The right-hand side of this equation is the numerical dissipation

$$\varepsilon_{num}(\boldsymbol{\xi}) = \widehat{\boldsymbol{G}}^{-1}(\boldsymbol{\xi})\widehat{\boldsymbol{u}}_C^*(\boldsymbol{\xi})\cdot\widehat{\boldsymbol{\mathcal{G}}}_C(\boldsymbol{\xi}) \tag{12}$$

implied by the discretization of the convective term. Now we investigate how to model the physical subgrid dissipation ε_{SGS} by ε_{num}.

An exact match between ε_{num} and ε_{SGS} cannot be achieved since ε_{SGS} involves interactions with non-represented scales. For modeling it is therefore necessary to invoke theoretical energy-transfer expressions. Employing an eddy-viscosity hypothesis the subgrid-scale dissipation is

$$\varepsilon_{SGS}(\boldsymbol{\xi}) = 2\nu_{SGS}\xi^2\widehat{E}(\boldsymbol{\xi}) \tag{13}$$

Similarly, the numerical dissipation can be expressed as

$$\nu_{num} = \frac{\varepsilon_{num}(\boldsymbol{\xi})}{2\xi^2\widehat{E}(\boldsymbol{\xi})}\ . \tag{14}$$

In general ν_{num} is a function of the wavenumber vector $\boldsymbol{\xi}$. For isotropic turbulence, however, statistical properties of eq. (11) follow from the scalar evolution equation for the 3D energy spectrum

$$\frac{\partial \widehat{E}(\xi)}{\partial t} - \widehat{T}_C(\xi) + 2\nu\xi^2\widehat{E}(\xi) = \varepsilon_{num}(\xi) \tag{15}$$

This equation is obtained from eq. (11) by integration over spherical shells with radius $\xi = |\boldsymbol{\xi}|$

$$\widehat{\varphi}(\xi) = \oint_{|\boldsymbol{\xi}|=\xi}\widehat{\varphi}(\boldsymbol{\xi})d\boldsymbol{\xi} \tag{16}$$

For a given numerical scheme $\nu_{num}(\xi)$ can be computed from

$$\nu_{num}(\xi) = -\frac{\widehat{G}^{-1}(\xi)}{2\xi^2\widehat{E}(\xi)}\int_{|\boldsymbol{\xi}|=\xi}\widehat{\boldsymbol{u}}_C^*(\boldsymbol{\xi})\cdot\widehat{\boldsymbol{\mathcal{G}}}_N(\boldsymbol{\xi})d\boldsymbol{\xi} \tag{17}$$

Convenient for our purposes is a normalization by

$$\nu_{num}^+(\xi^+) = \nu_{num}\ \ \frac{\xi}{\xi_C}\ \ \sqrt{\frac{\xi_C}{\widehat{E}(\xi_C)}} \tag{18}$$

with $\xi^+ = \frac{\xi}{\xi_C}$.

The concept of a wavenumber-dependent spectral eddy viscosity was first proposed by Heisenberg (1946). For high Reynolds numbers and under the assumption of a Kolmogorov range $E(\xi) = C_K\varepsilon^{3/2}\xi^{-5/3}$ extending to infinity the Eddy-Damped Quasi-Normal Markovian (EDQNM) theory (Lesieur 1997) leads to

$$\nu_{SGS}^+(\xi^+) = 0.441C_K^{-3/2}X(\xi^+) \tag{19}$$

where $X(\xi^+)$ is a non-dimensional function exhibiting a plateau at unity for small wavenumbers $\xi^+ \lesssim 1/3$ and a

sharply rising cusp in the vicinity of the cut-off wave number $\xi^+ = 1$. Chollet (1984) proposes the expression

$$\nu^+_{Chollet}(\xi^+) = 0.441 C_K^{-3/2} \quad 1 + 34.47 e^{3.03\xi^+} \tag{20}$$

as best fit to the exact solution.

In the following the objective is to adjust the free parameters of the implicit model to make its dissipative properties consistent with analytical theories of turbulence. For this purpose we consider a numerical simulation of freely decaying homogeneous isotropic turbulence in the limit of vanishing molecular viscosity. The computational domain is a $(2\pi)^3$-periodic box, discretized by $32 \times 32 \times 32$ uniform finite volumes. Filtered and truncated highly resolved LES data are used as initial condition $\bar{\boldsymbol{u}}_N(t_0)$. Solutions $\bar{\boldsymbol{u}}_N(t_n)$ at time $t_n = t_0 + n\Delta t$, n being an integer, are obtained by advancing n time steps with ALDM. An *a-posteriori* analysis of the data allows to identify the spectral eddy viscosity of the implicit SGS model. For this purpose an algorithm proposed by Domaradzki et al. (2003) is adapted.

The computed velocity fields $\bar{\boldsymbol{u}}_N(t_n)$ are Fourier-transformed and truncated at $\xi_C = 15$. Energy spectra $\widehat{E}(\boldsymbol{\xi}, t_n)$ and spectral transfer functions $\widehat{T}_C(\boldsymbol{\xi}, t_n)$ are computed from equations (8) and (10). The convolution integral in eq. (10) is computed in real space. The computation of the numerical-dissipation spectrum, eq. (11) and (12), involves the spectral-energy decay which is approximated by

$$\frac{\partial \widehat{E}(\boldsymbol{\xi}, t_{n-1/2})}{\partial t} \approx \frac{\widehat{E}(\boldsymbol{\xi}, t_n) - \widehat{E}(\boldsymbol{\xi}, t_{n-1})}{\Delta t} \tag{21}$$

at times $t_{n-1/2} = \frac{1}{2}(t_{n-1} + t_n)$. Energy spectrum and spectral transfer function are interpolated as

$$\widehat{E}(\boldsymbol{\xi}, t_{n-1/2}) = \frac{\widehat{E}(\boldsymbol{\xi}, t_n) + \widehat{E}(\boldsymbol{\xi}, t_{n-1})}{2} \tag{22a}$$

$$\widehat{T}_C(\boldsymbol{\xi}, t_{n-1/2}) = \frac{\widehat{T}_C(\boldsymbol{\xi}, t_n) + \widehat{T}_C(\boldsymbol{\xi}, t_{n-1})}{2} \tag{22b}$$

Following eqs. (11,12,14) the spectral numerical viscosity is

$$\nu_{num}(\boldsymbol{\xi}, t_{n-1/2}) = \frac{\widehat{T}_C(\boldsymbol{\xi}, t_{n-1/2}) - \frac{\partial \widehat{E}(\boldsymbol{\xi}, t_{n-1/2})}{\partial t}}{2\boldsymbol{\xi}^2 \widehat{E}(\boldsymbol{\xi}, t_{n-1/2})} - \nu \tag{23}$$

The 3D numerical-viscosity spectrum is obtained by averaging over integer-wavenumber shells $\xi - \frac{1}{2} \le |\boldsymbol{\xi}| \le \xi + \frac{1}{2}$

$$\nu_{num}(\xi, t_{n-1/2}) = \frac{4\pi\xi^2}{M(\xi)} \sum_{\boldsymbol{\xi}} \nu_{num}(\boldsymbol{\xi}, t_{n-1/2}) \tag{24}$$

where $M(\xi)$ is the number of integer wavenumbers on each shell with radius ξ. A subsequent normalization gives

$$\nu^+_{num}(\xi^+, t_{n-1/2}) = \nu_{num}(\xi_C \xi^+, t_{n-1/2}) \sqrt{\frac{\xi_C}{\widehat{E}(\xi_C)}} \tag{25}$$

Isotropic decaying turbulence does not loose memory of the initial data. An evaluation of ν^+_{num} for one data set only does not necessarily represent the statistical average. To cope with this problem the spectral numerical viscosity from 10 uncorrelated realizations is evaluated and averaged. Each realization is advanced by one time step so that computational cost amounts to 10 time steps per evaluated numerical viscosity. This evaluation procedure is sufficiently efficient for an automatic optimization of the free parameter values of the discretization scheme.

As cost function we define the root-mean-square difference between the spectral numerical viscosity $\nu^+_{num}(\xi^+)$ and the spectral eddy viscosity $\nu^+_{Chollet}(\xi^+)$ of EDQNM.

The employed automatic optimization algorithm follows an evolutionary strategy which models natural biological processes by stochastic search methods. A set of parameters is considered as genome of a living individual. The algorithm operates on a population of individuals and is therefore particularly suitable for non-smooth cost functions. It applies the survival-of-the-fittest principle of the Darwinian theory of evolution. At each generation a new set of individuals is created by modeled natural processes, such as selection, recombination, and random mutation. This process leads to a population of individuals that is better adapted to a cost function than the population that it was created from. For further details the reader is referred to Adams et al. (2004), Hickel et al. (2004) and the references therein.

After an evaluation of 200 generations, each with 50 individuals, a final set of parameters was selected. As shown by Hickel et al. (2005) the spectral eddy viscosity of the ALDM scheme with these parameters yields an excellent match with theoretical predictions, figure 1. It exhibits a low-wavenumber plateau at the correct magnitude and and recovers the typical cusp in the vicinity of the cut-off wave number.

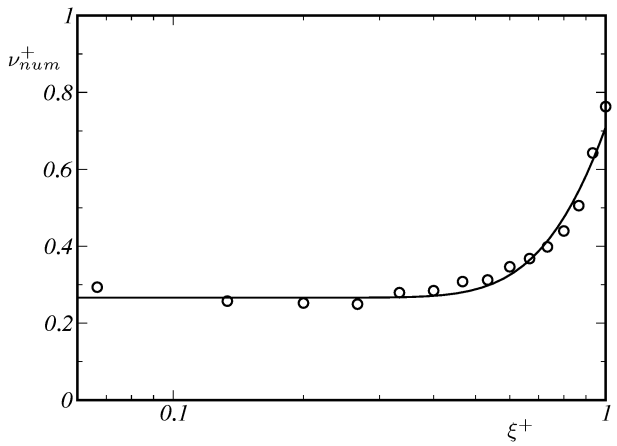

Figure 1: Numerical viscosity of ALDM with optimized parameters compared to the prediction of turbulence theory. ∘ ALDM, —— EDQNM theory (Chollet, 1984).

VALIDATION

For *a posteriori* validation of the implicit SGS model provided by ALDM we perform LES of large-scale forced and of decaying isotropic turbulence.

All simulations presented in this section are carried out in a $(2\pi)^3$-periodic computational domain. The computational domain is discretized by 64^3 cells unless specified otherwise. For time advancement, we use an explicit third-order Runge-Kutta scheme of Shu (1988). The time step Δt is adjusted dynamically according to the Courant-Friedrichs-Lewy limit with CFL = 1.0.

Forced homogeneous isotropic turbulence

For the first test case a large-scale force is added to the right-hand side of the momentum equation. This extra source term results in a production of kinetic energy at large scales that compensates dissipation. Scales smaller than $\xi_S = 3$ remain unaffected.

We perform simulations for four different cases corresponding to the combination of two different grids with two different Reynolds numbers. The computational domain is a $(2\pi)^3$-periodic box. The coarser grid is composed of $N^3 = 32^3$, the finer one of $N^3 = 64^3$ evenly-spaced cells. The computational Reynolds numbers $Re = 1/\nu$ are $Re = 10^2$ and $Re = 10^5$. For the lower Reynolds number the Kolmogorov length scale is of the order of the mesh size $\Delta x = 2\pi/N$ for $N = 64$. The initial condition is a divergence-free velocity field with random phases and with a 3D energy spectrum $\widehat{E}(\xi) = \frac{1}{2}\xi^{-5/3}$. After an initial transient of 50 time steps samples of the 3D energy spectra were collected until a converged mean spectrum was observed.

The resulting 3D energy spectra are shown in figure 2. For $Re = 10^2$ the largest resolved wave numbers are within the dissipative range. For this case the isotropic Taylor micro scale λ_T can be approximated in terms of the resolved 3D energy spectrum (McComb 1990). We obtain a micro-scale Reynolds number $Re_\lambda = 78$ with $N = 32$ and $Re_\lambda = 73$ with $N = 64$. For $Re = 10^5$ the 3D mean energy spectra coincide for both mesh resolutions and follow the Kolmogorov law. This result verifies a posteriori the optimum parameter set which was based on the corresponding theoretical prediction.

We conclude that with the model parameters found by an optimum match of a theoretical prediction for isotropic turbulence at $Re \to \infty$ the SGS dissipation predicted by ALDM correctly models the local energy transfer. This holds for cut-off wavenumbers ξ_C within the inertial range and even for lower Reynolds numbers, for which ξ_C is in the dissipative range. This indicates that the used model parameters may be valid universally. This is investigated in the following sections, where the parameter set is kept unchanged.

Isotropic turbulence at $Re \longrightarrow \infty$

We integrate the Navier-Stokes equation by initially prescribing $\widehat{E}(\xi)$ as inertial-range spectrum for homogeneous isotropic turbulence in the limit $Re \longrightarrow \infty$. After an initial transient during which the initial randomly oriented phases re-align by Navier-Stokes dynamics the energy spectrum decays self-similarly while preserving the $\xi^{-5/3}$ law up to the largest wavenumbers, see fig. 3. The observed decay rate $\varepsilon = -\partial K/\partial t$ of the resolved turbulent kinetic energy

$$K(t) = \sum_{1}^{\xi_C} \widehat{E}(\xi, t) \tag{26}$$

is proportional to the turbulent kinetic energy to the power of 3/2, see fig. (4), as required for self-similar decay of an inertial-range spectrum.

Decay rate and energy-spectrum shape can be assessed simultaneously by the Kolmogorov function

$$C_K(\xi, t) = \varepsilon(t)^{-2/3}\ \xi^{5/3}\ \widehat{E}(\xi, t) \tag{27}$$

which is plotted in figure 5. For an idealized setting the Kolmogorov function would be constant. For our simulations we find a $C_K(\xi, t)$ which is almost constant in time and has a wide plateau in ξ at $C_K \approx 1.8$. This value slightly differs from theoretical predictions, but is in reasonable agreement with other published results. A comprehensive account of the value of the Kolmogorov constant in numerical simulations of isotropic turbulence is given by Yeung and Zhou (1997).

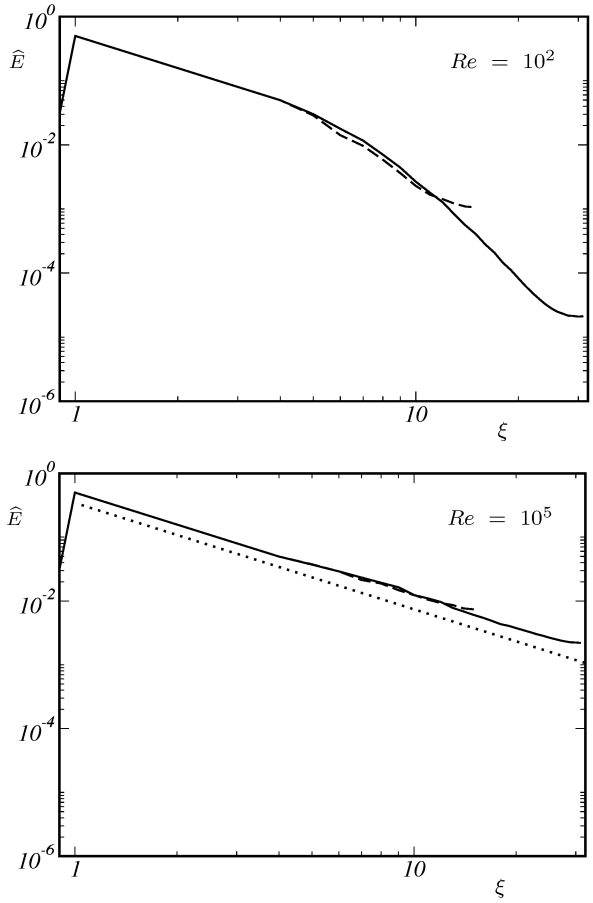

Figure 2: Mean 3D energy spectra for LES of the large-scale forced Navier-Stokes equation; ——— with 64^3 cells; – – – – with 32^3 cells; · · · · · line $\sim \xi^{-5/3}$.

Comte-Bellot – Corrsin experiment

A more complex situation is encountered for decaying grid-generated turbulence for which also the correct representation of the energy-containing range of the spectrum is important (Pope 2000). Computations are initialized with spectrum and Reynolds numbers adapted to the wind-tunnel experiments of Comte-Bellot and Corrsin (1971), denoted hereafter as CBC. Among other space-time correlations CBC provides streamwise energy spectra for grid-generated turbulence at three positions downstream of a mesh with a width $M = 5.08$cm. Table 3 of Comte-Bellot and Corrsin (1971) gives corresponding 3D energy spectra which were obtained under the assumption of isotropy.

In the simulation this flow is modeled by moving the $(2\pi)^3$-periodic computational domain downstream with the mean flow speed. The energy distribution of the initial velocity field is matched to the first measured 3D energy spectrum

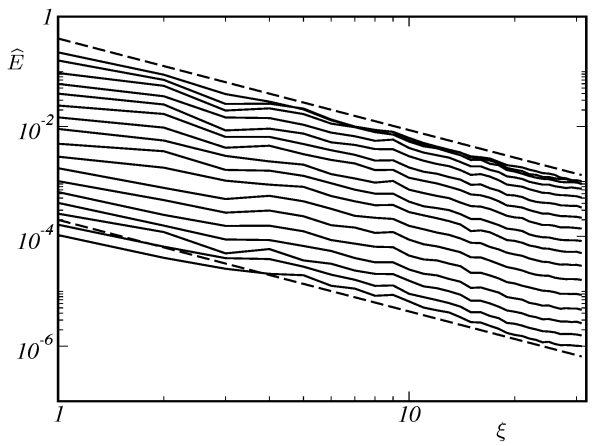

Figure 3: Instantaneous 3D energy spectra for LES of decaying homogeneous isotropic turbulence at the inviscid limit. —— instantaneous spectra ; – – – – $\widehat{E} \sim \xi^{-5/3}$.

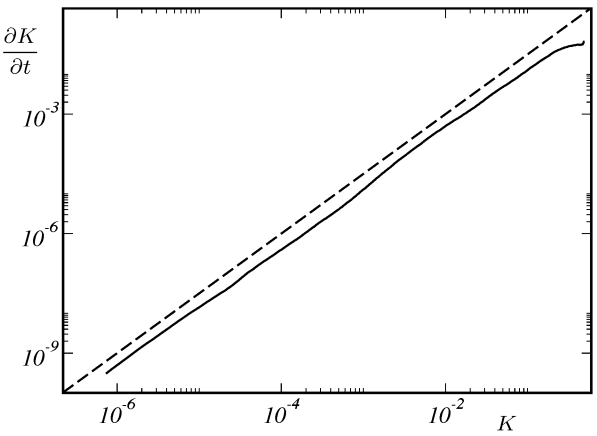

Figure 4: Phase diagram of turbulent kinetic energy for decaying homogeneous isotropic turbulence at $Re \longrightarrow \infty$. – – – – $\varepsilon \sim K^{3/2}$.

of CBC. The SGS model can now be verified by comparing computational and experimental 3D energy spectra at later time instants which correspond to the other two measuring stations.

The experimental data are non-dimensionalized as proposed by Misra and Lund (1996) and by Ghosal et al. (1995). In order to create the initial velocity field a random field was allowed to develop for about one large-eddy turnover time according to Navier-Stokes dynamics while maintaining the 3D energy spectrum as given for the first measuring station.

Results of ALDM are compared with those obtained with a 4th-order central discretization scheme and an explicit Smagorinsky SGS model. The Smagorinsky model is used in its conventional and in its dynamic version. For the conventional model (Smagorinsky 1963) the parameter is set to $C_S = 0.18$. Lilly (1967) derived this value for sufficiently large Reynolds numbers and a sharp spectral cut off in the inertial range assuming $C_K \approx 1.4$. The dynamic algorithm was proposed by Germano et al. (1991). Here, C_S is computed according to Lilly (1992), and an average over the entire flow

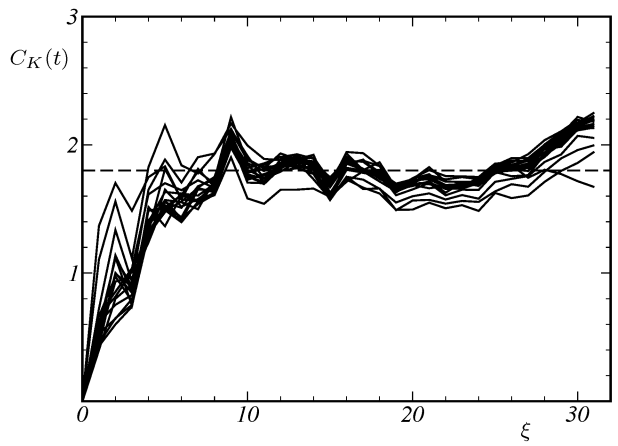

Figure 5: Kolmogorov function for decaying homogeneous isotropic turbulence at $Re \longrightarrow \infty$. – – – – $C_K = 1.8$.

field is taken to prevent local numerical instabilities, as it is established standard.

Examining the computed energy spectra, figure 7, we note that ALDM performs just as well as the dynamic Smagorinsky SGS model. It should be noted that the prediction of the dynamic Smagorinsky model can be associated as a reference for isotropic turbulence. The conventional Smagorinsky model requires ad-hoc adjustment of C_S. We have observed, that choosing C_S somewhat smaller than the theoretical value gives better results which are close to those of the dynamic Smagorinsky model.

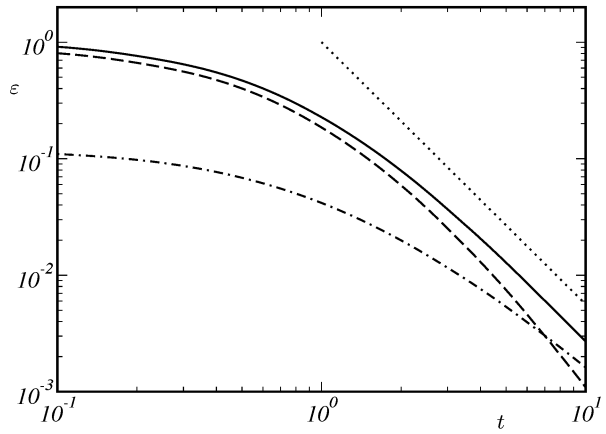

Figure 6: Contributions to energy dissipation in ALDM for LES of decaying homogeneous isotropic turbulence according to the Comte-Bellot – Corrsin experiment ; – · – · – molecular dissipation, – – – – implicit SGS dissipation, —— total dissipation, · · · · · $\varepsilon \sim t^{-2.25}$.

For the decay of total kinetic energy K, figure 6, we find $\partial K/\partial t \sim t^{-n}$ with $n = 1.25$. This corresponds to $\varepsilon = \partial K/\partial t \sim t^{-2.25}$ or $\varepsilon \sim K^{1.8}$. The exponent $n = 1.25$ is in a reasonable agreement with published experimental data (AGARD 1998; Comte-Bellot and Corrsin 1971; Kang, Chester, and Meneveau 2003) which range from $n = 1.2$ to $n = 1.3$.

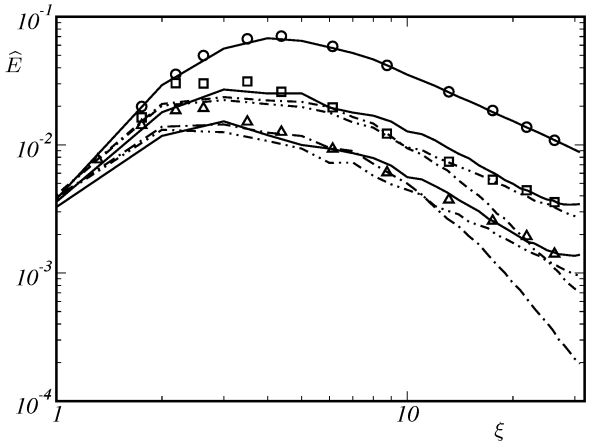

Figure 7: Instantaneous 3D energy spectra for LES with 64^3 cells and for measurements of Comte-Bellot – Corrsin ; – · – · – Smagorinsky model, – · · – · · dynamic Smagorinsky model, ——— ALDM ; ◯ $t' = 42$, □ $t' = 98$ and △ $t' = 171$ experimental data of Comte-Bellot and Corrsin (1971).

CONCLUSION

With the implicit LES approach the truncation error of the discretization of the nonlinear terms functions as a SGS model. Therefore, an explicit computation of model expressions is unnecessary. The presented approach which we refer to as ALDM is based on an adaptive local deconvolution operator which introduces SGS model parameters directly into the discretization scheme. A spectral-space analysis of the modified differential equation is employed to compare the effective spectral numerical viscosity of ALDM with theoretical predictions for isotropic turbulence. By means of an evolutionary optimization algorithm a set of parameters is found which gives an excellent match with the spectral eddy viscosity predicted by EDQNM theory. Computational results are provided for different large-scale forced and decaying fully turbulent flow configurations with periodic boundary conditions. It is demonstrated that ALDM performs as well as established explicit models. The application of ALDM to wall-bounded flows is subject of ongoing research.

ACKNOWLEDGMENTS The presented research is supported by the German Research Council (DFG) in the framework of the French-German research group "LES of Complex Flows" (FG507). J.A. Domaradzki was supported by NSF and a research fellowship of the Alexander von Humboldt Foundation.

REFERENCES

Adams, N. A., S. Hickel, and S. Franz (2004). Implicit subgrid-scale modeling by adaptive deconvolution. *J. Comput. Phys. 200*, 412–431.

AGARD (1998). *A Selection of Test Cases for the Validation of Large-Eddy Simulations of Turbulent Flows*. Technical Report AGARD-AR-345. NATO.

Chollet, J. P. (1984). Two-point closures as a subgrid-scale modeling tool for large-eddy simulations. In F. Durst and B. E. Launder (Eds.), *Turbulent Shear Flows IV*, Heidelberg, pp. 62–72. Springer.

Comte-Bellot, G. and S. Corrsin (1971). Simple Eulerian time correlation of full and narrow-band velocity signals in grid-generated 'isotropic' turbulence. *J. Fluid Mech. 48*, 273–337.

Domaradzki, J. A., Z. Xiao, and P. K. Smolarkiewicz (2003). Effective eddy viscosities in implicit large eddy simulations of turbulent flows. *Phys. Fluids 15*, 3890–3893.

Germano, M., U. Piomelli, P. Moin, and W. H. Cabot (1991). A dynamic subgrid-scale eddy viscosity model. *Phys. Fluids A 3*, 1760–1765.

Ghosal, S. (1996). An analysis of numerical errors in large-eddy simulations of turbulence. *J. Comput. Phys. 125*, 187–206.

Ghosal, S., T. S. Lund, P. Moin, and K.Akselvoll (1995). A dynamic localization model for large-eddy simulation of turbulent flows. *J. Fluid Mech. 286*, 229–255.

Grinstein, F. F. and C. Fureby (2004). From canonical to complex flows: recent progress on monotonically integrated LES. *Comp. Sci. Eng. 6*, 36–49.

Heisenberg, W. (1946). Zur statistischen Theorie der Turbulenz. *Z. Phys. 124*, 628–657.

Hickel, S., N. A. Adams, and J. A. Domaradzki (2005). An adaptive local deconvolution method for implicit LES. *J. Comput. Phys.*, (submitted).

Hickel, S., S. Franz, N. Adams, and P. Koumoutsakos (2004). Optimization of an implicit subgrid-scale model for LES. In *Proceedings of the 21st International Congress of Theoretical and Applied Mechanics*, Warsaw, Poland.

Kang, H. S., S. Chester, and C. Meneveau (2003). Decaying turbulence in an active-grid-generated flow and large-eddy simulation. *J. Fluid Mech. 480*, 129–160.

Leonard, A. (1974). Energy cascade in large eddy simulations of turbulent fluid flows. *Adv. Geophys. 18A*, 237–248.

Lesieur, M. (1997). *Turbulence in Fluids* (3 ed.). Dordrecht, The Netherlands: Kluwer Academic Publishers.

Lilly, D. K. (1967). The representation of small-scale turbulence in numerical simulation experiments. In H. H. Goldstein (Ed.), *Proc. IBM Scientific Computing Symposium on Environmental Sciences*, pp. 195–201. IBM.

Lilly, D. K. (1992). A proposed modification of the Germano subgrid-scale closure model. *Phys. Fluids A 4*, 633–635.

McComb, W. D. (1990). *The Physics of Fluid Turbulence*. Oxford: Clarendon Press.

Misra, A. and T. S. Lund (1996). Evaluation of a vortex-based subgrid stress model using DNS databases. In *CTR Proc. 1996 Summer Program*, Stanford, California, pp. 359–368. Center for Turbulence Research,Stanford University and NASA Ames Research Center.

Pope, S. B. (2000). *Turbulent Flows*. Cambridge University Press.

Shu, C.-W. (1988). Total-variation-diminishing time discretizations. *SIAM J. Sci. Stat. Comput. 9*(6), 1073–1084.

Smagorinsky, J. (1963). General circulation experiments with the primitive equations. *Mon. Weath. Rev. 93*, 99–164.

Yeung, P. K. and Y. Zhou (1997). On the universality of the Kolmogorov constant in numerical simulations of turbulence. Technical Report 97-64, ICASE, NASA Langley Research Center, Hampton, Virginia.